



Comparative measurements of inverse spin Hall effects and magnetoresistance in YIG/Pt and YIG/Ta

C. Hahn, G. de Loubens,* O. Klein, and M. Viret

Service de Physique de l'État Condensé (CNRS URA 2464), CEA Saclay, 91191 Gif-sur-Yvette, France

V. V. Naletov

*Service de Physique de l'État Condensé (CNRS URA 2464), CEA Saclay, 91191 Gif-sur-Yvette, France and
Institute of Physics, Kazan Federal University, Kazan 420008, Russian Federation*

J. Ben Youssef

Université de Bretagne Occidentale, Laboratoire de Magnétisme de Bretagne CNRS, 6 Avenue Le Gorgeu, 29285 Brest, France

(Received 18 February 2013; published 13 May 2013)

We report on a comparative study of spin Hall related effects and magnetoresistance in YIG|Pt and YIG|Ta bilayers. These combined measurements allow to estimate the characteristic transport parameters of both Pt and Ta layers juxtaposed to yttrium iron garnet (YIG): the spin mixing conductance $G_{\uparrow\downarrow}$ at the YIG|normal metal interface, the spin Hall angle Θ_{SH} , and the spin diffusion length λ_{sd} in the normal metal. The inverse spin Hall voltages generated in Pt and Ta by the pure spin current pumped from YIG excited at resonance confirm the opposite signs of spin Hall angles in these two materials. Moreover, from the dependence of the inverse spin Hall voltage on the Ta thickness, we extract the spin diffusion length in Ta, found to be $\lambda_{\text{sd}}^{\text{Ta}} = 1.8 \pm 0.7$ nm. Both the YIG|Pt and YIG|Ta systems display a similar variation of resistance upon magnetic field orientation, which can be explained in the recently developed framework of spin Hall magnetoresistance.

DOI: [10.1103/PhysRevB.87.174417](https://doi.org/10.1103/PhysRevB.87.174417)

PACS number(s): 85.75.-d, 76.50.+g

I. INTRODUCTION

Spintronics aims at designing devices that capitalize on the interplay between the spin and charge degrees of freedom of the electron. In particular, it is of central interest to study the interconversion from a spin current, the motion of spin angular momentum, to a charge current and the transfer of spin angular momentum between the conduction electrons of a normal metal (NM) and the magnetization of a ferromagnetic material (FM). The separation of oppositely spin-polarized electrons of a charge current through spin-orbit coupling is called spin Hall effect (SHE).^{1,2} Its inverse process (ISHE) converts spin currents into charge currents and has recently sparked an intense research activity,^{3,4} as it allows for an electrical detection of the dynamical state of a ferromagnet.^{5,6} Indeed, a precessing magnetization in a ferromagnet generates a spin current via spin pumping,⁷ which can be converted, at the interface with an adjacent normal layer, to a dc voltage by ISHE. Moreover, electronic transport can also be affected by the static magnetization in the FM as electrons spins separated by SHE can undergo different spin-flip scattering on the interface with the FM layer. In particular, spin-flipped electrons are deflected by ISHE in a direction opposite to the initial current, leading to a reduced total current at constant voltage. This effect depends on the relative orientation between magnetization and current direction, and has recently been called spin Hall magnetoresistance (SMR).⁸

Experimental studies on spin pumping induced inverse spin Hall voltages (V_{ISH}) in FM|NM bilayers were first carried out with Pt as NM in combination with NiFe as FM^{5,9-12} and more recently with the insulating ferrimagnet yttrium iron garnet (YIG).^{6,13-17} Although other strong spin-orbit metals have been tried in combination with the metallic ferromagnets

NiFe^{18,19} and CoFeB,^{20,21} inverse spin Hall voltage^{6,17} and magnetoresistance^{8,22} measurements made on YIG|NM have so far been limited to NM = Pt. Still, it would be very interesting to compare V_{ISH} and SMR measurements on different YIG|NM systems, including metals having opposite spin Hall angles, such as Pt versus Ta.^{20,23} *Ab initio* calculations indeed predict the spin Hall angle of the resistive β phase of Ta to be larger and of opposite sign to that of Pt.²⁴ The defining parameters for V_{ISH} and SMR are the spin diffusion length in the normal metal, λ_{sd} , the spin Hall angle Θ_{SH} , which quantifies the efficiency of spin to charge current conversion, and the spin mixing conductance ($G_{\uparrow\downarrow}$), which depends on the scattering matrices for electrons at the FM|NM interface⁷ and can be seen as the transparency of the interface for transfer of spin angular momentum.²⁵ The evaluation of the three above mentioned parameters is a delicate task,²⁶ as the measured V_{ISH} voltages and SMR ratio depend on all of them.

In this paper, we present a comparative study of YIG|Pt and YIG|Ta bilayers, where we measure both the ISHE and SMR on each sample. We confirm the opposite signs of spin Hall angles in Pt and Ta and the origin of SMR, which has been explained in Ref. 8. Thanks to these combined measurements, we can evaluate the spin mixing conductances of the YIG|Pt and YIG|Ta interfaces and the spin Hall angles in Pt and Ta. In order to get more insight on the previously unexplored YIG|Ta system, we study the dependence of ISHE on Ta film thickness, which enables us to extract the spin diffusion length in Ta.

The remaining of the manuscript is organized as follows. Section II gives details on the samples and experimental setup used in this study. In Sec. III, the experimental data of V_{ISH} and SMR obtained on the YIG|Pt and YIG|Ta systems are presented and analyzed. In Sec. IV, we discuss the transport parameters extracted from our measurements. We also

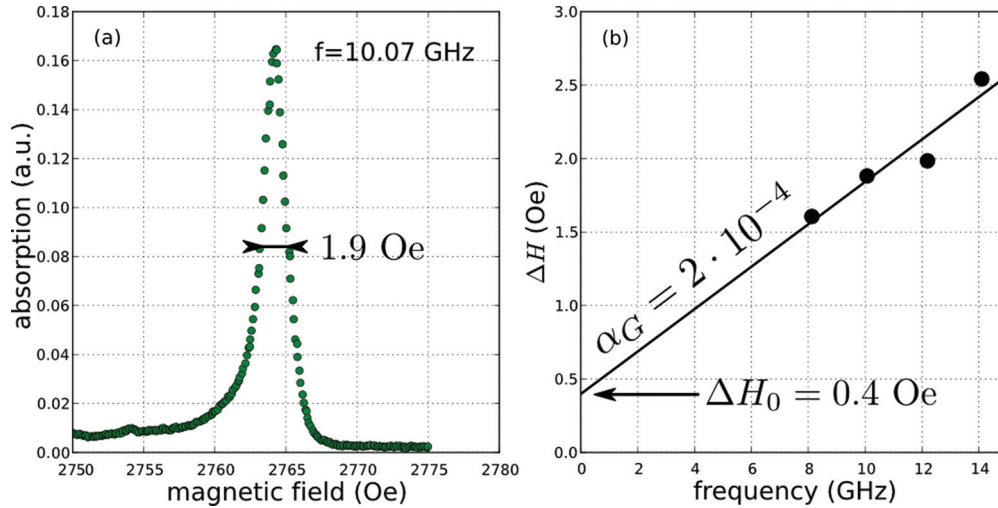


FIG. 1. (Color online) (a) Standard in-plane FMR spectrum of a bare YIG 200-nm thin film used in this study. (b) Full FMR linewidth vs frequency.

comment on the absence of direct effect of a charge current in Pt on the linewidth of our 200-nm-thick YIG samples. Finally, we emphasize the main results of this work in the conclusion.

II. EXPERIMENTAL DETAILS

A. Samples

1. YIG films

Two single-crystal $\text{Y}_3\text{Fe}_5\text{O}_{12}$ (YIG) films of 200-nm thickness were grown by liquid phase epitaxy on (111) $\text{Gd}_3\text{Ga}_5\text{O}_{12}$ (GGG) substrates,²⁷ and labeled YIG1 and YIG2. Epitaxial growth of the YIG was verified by x-ray diffraction and the films roughness was determined by atomic force microscopy to be below 5 Å. Their magnetic static properties were investigated by vibrating sample magnetometry. The in-plane behavior of the thin YIG films is isotropic with a coercivity below 0.6 Oe.²⁷ The saturation magnetization, found to be 140 emu/cm^3 , corresponds to the one of bulk YIG. This value was verified by performing ferromagnetic resonance (FMR) at different excitation frequencies.

FMR also allows to extract the magnetic dynamic properties of the 200-nm-thick YIG films. A typical FMR spectrum of the YIG1 film obtained at 10 GHz and low microwave power ($P = -20 \text{ dBm}$) is presented in Fig. 1(a). The gyromagnetic ratio of our YIG films is found to be $\gamma = 1.79 \times 10^7 \text{ rad/s/Oe}$. From the dependence of the linewidth on the excitation frequency, their Gilbert damping $\alpha_G = (2.0 \pm 0.2) \times 10^{-4}$ can be determined, see Fig. 1(b). This value highlights the very small magnetic relaxation of these thin films. Still, there is an inhomogeneous part to the linewidth [$\Delta H_0 = 0.4 \text{ Oe}$ in Fig. 1(b)]. For one of the two prepared films (YIG2), two to three closely spaced resonance lines could be observed in some cases, which we attribute to distinct sample regions having slightly different properties.

2. YIG|Pt and YIG|Ta bilayers

After these standard magnetic characterizations, the YIG films were cut into slabs with lateral dimensions of

$1.1 \text{ mm} \times 7 \text{ mm}$ in order to perform inverse spin Hall voltage and magnetoresistance measurements. Platinum and tantalum thin films were then grown by rf sputter deposition, at a power density of 4 W/cm^2 . The growth of the resistive β phase of Ta was achieved by optimizing the Ar pressure during the sputtering process. This study was conducted in parallel onto oxidised Si and GGG(111) substrates. The appearance of the tetragonal crystalline phase in a narrow window around 10^{-2} mbar was verified by the presence of the characteristic (200)- β -Ta line in the x-ray diffraction spectra.²⁸ The β phase was also confirmed by the resistivity of the films,²⁰ which for 10-nm Ta thickness lies at $200 \mu\Omega \text{ cm}$.

In order to compare ISHE and SMR on YIG|Pt and YIG|Ta bilayers, a 15-nm-thick Pt and a 3-nm-thick Ta layers were grown on the YIG1 sample. The conductivities of these metallic films are $\sigma^{\text{Pt}} = 2.45 \times 10^6 \Omega^{-1} \text{ m}^{-1}$ (in agreement with the values reported in Refs. 17 and 18) and $\sigma^{\text{Ta}} = 3.05 \times 10^5 \Omega^{-1} \text{ m}^{-1}$, respectively. These two samples have been used to obtain the results presented in Figs. 2 and 4. The dependence on Pt thickness of both V_{ISH} ¹⁷ and magnetoresistance^{22,29} has been studied earlier. In this work, we have used the YIG2 sample to study the dependence as a function of the Ta thickness, which was varied from 1.5 to 15 nm (1.5, 2, 3, 5, 10, and 15 nm). The conductivity of these Ta films increases from 0.8×10^5 to $7.5 \times 10^5 \Omega^{-1} \text{ m}^{-1}$ with the film thickness. This series of samples has been used to obtain the data of Fig. 3. Finally, Pt films with thicknesses 10 and 15 nm were also grown on YIG2, for the sake of comparison with YIG1.

B. Measurement setup

A 500- μm -wide and 2- μm -thick Au transmission line cell and electronics providing frequencies up to 20 GHz were used for microwave measurements. The long axis of the sample was aligned perpendicularly to the microwave line, thus parallel to the excitation field h_{rf} as indicated in the inset of Fig. 2. V_{ISH} was measured by a lock-in technique (with the microwave power turned on and off at a frequency of a few kilohertz) with electrical connections through gold leads

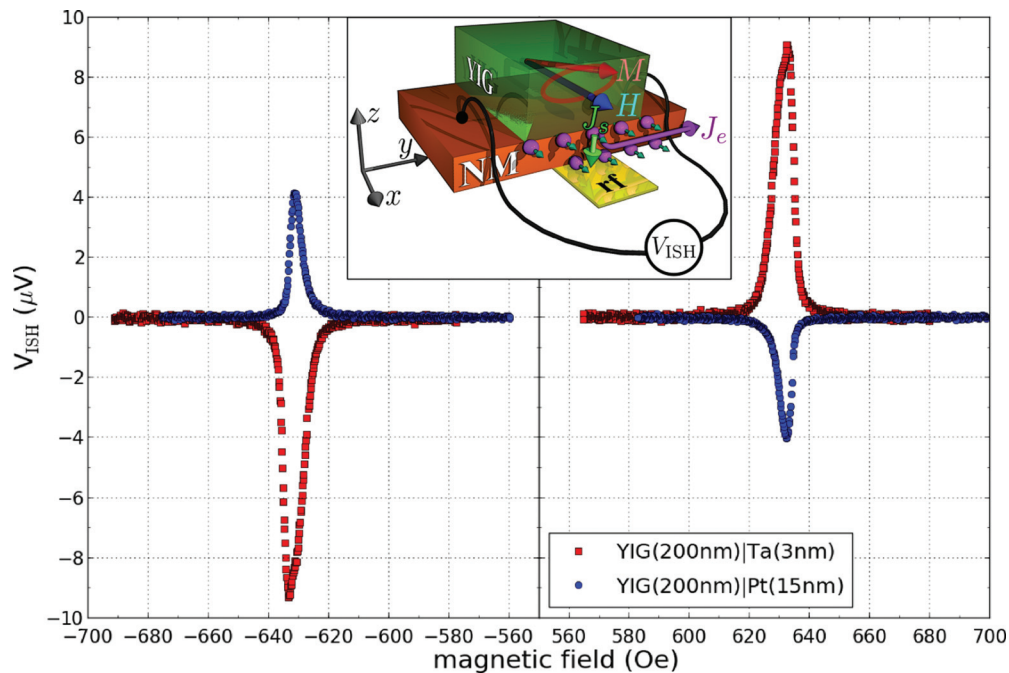


FIG. 2. (Color online) Inverse spin Hall voltage measured at 3.5 GHz for YIG|Ta and YIG|Pt. (Inset) Sketch of the experiment.

at equal distance to the area of excitation. Magnetotransport measurements of the YIG|NM slabs were performed using a four-point configuration. The samples were placed at the center of an electromagnet, which can be rotated around its axis in order to obtain curves of magnetoresistance versus angle. The measurement cell was placed in a cryostat, with the possibility to cool down to 77 K. All the measurements presented in this paper were performed at room temperature, except for those reported in Fig. 5.

III. EXPERIMENTAL RESULTS AND ANALYSIS

A. Inverse spin Hall voltage: YIG|Pt versus YIG|Ta

First, we compare in Fig. 2 the inverse spin Hall voltages measured at 3.5 GHz ($P = +10$ dBm) in the YIG|Pt and YIG|Ta bilayers. It shows that one can electrically detect the FMR of YIG in these hybrid systems.⁶ The spin current J_s pumped into the adjacent normal metal by the precessing magnetization in YIG is converted into a charge current by ISHE,

$$J_e = \frac{2e}{\hbar} \Theta_{\text{SH}} J_s, \quad (1)$$

where e is the electron charge and \hbar the reduced Planck constant. This leads to a transverse voltage V_{ISH} (across the length of the YIG|NM slab), as sketched in the inset of Fig. 2. Moreover, V_{ISH} must change sign upon reversing the magnetization of YIG because of the concomitant reversal of the spin pumped current J_s (hence J_e). This is observed in both the YIG|Pt and YIG|Ta systems, where V_{ISH} is odd in applied magnetic field, which shows that the voltage generated at resonance is not due to a thermoelectric effect.

The striking feature to be observed here is the opposite signs of V_{ISH} in these two samples. This remains true at all microwave frequencies (from 2 to 8 GHz) and power levels (from -8 to $+10$ dBm), which were measured, as well as

for the different YIG|Pt and YIG|Ta bilayers made from YIG1 and YIG2 samples. It thus confirms that the spin Hall angles in Ta and Pt have opposite signs, as predicted by *ab initio* calculations²⁴ and inferred from measurements where the spin current was generated by a metallic ferromagnet.^{20,23} Moreover, from the electrical circuit that was used in the measurements (the anode of the voltmeter is on the left in Fig. 2, inset), it can be found that $\Theta_{\text{SH}}^{\text{Pt}} > 0$, while $\Theta_{\text{SH}}^{\text{Ta}} < 0$. The precise estimation of the spin Hall angles in these two materials requires the extra analyses presented in the following sections. Still, it is interesting to note that the $4 \mu\text{V}$ amplitude of V_{ISH} measured in Fig. 2 on our 15-nm-thick Pt is close to the one reported in Ref. 17 (2 to $3 \mu\text{V}$) with comparable experimental conditions.

B. Dependence of inverse spin Hall voltage on Ta thickness

In this work, we have measured the dependence of V_{ISH} only on Ta thickness. The study as a function of Pt thickness was already reported in Ref. 17, using a similar 200-nm-thick YIG film (fabricated in the same laboratory). In Fig. 3, we have plotted using red squares the dependence of V_{ISH} on the Ta thickness measured on the series of samples described above. Here, V_{ISH} is produced by the precession of magnetization in YIG, resonantly excited at 3.8 GHz by the microwave field ($P = +10$ dBm). V_{ISH} increases from less than $2 \mu\text{V}$ up to $70 \mu\text{V}$ as the Ta layer thickness is reduced from 15 to 2 nm at which the maximal voltage is measured. For the thinnest Ta layer ($t_{\text{Ta}} = 1.5$ nm), V_{ISH} drops to about $10 \mu\text{V}$, a value close to the one observed at $t_{\text{Ta}} = 10$ nm. A similar dependence of V_{ISH} on Pt thickness was reported in Ref. 17, where a maximum of voltage was observed between $t_{\text{Pt}} = 1.5$ nm and $t_{\text{Pt}} = 6$ nm.

The resistance measured across the length of the YIG|Ta slab is also plotted with green crosses in Fig. 3 as a function of t_{Ta} (see right scale). It is interesting to note that both V_{ISH}

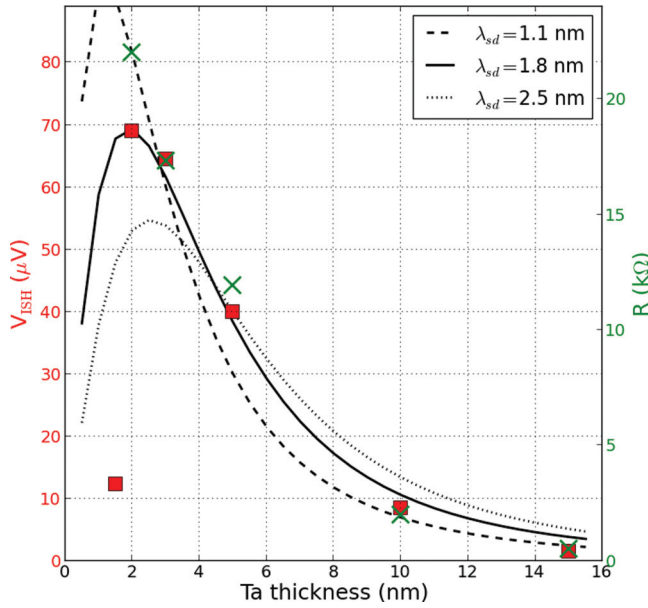


FIG. 3. (Color online) Dependence of inverse spin Hall voltage on Ta thickness (red squares, left scale). The microwave frequency is 3.8 GHz ($P = +10$ dBm). The lines are theoretical predictions¹⁷ from Eq. (2) for different values of λ_{sd} , with the parameters $G_{\uparrow\downarrow} = 4.3 \times 10^{13} \Omega^{-1} \text{m}^{-2}$ and $\Theta_{SH} = -0.02$. The resistance of the samples is also displayed (green crosses, right scale). The resistance of the 1.5-nm-thin Ta sample (95 k Ω) is out of range.

and R follow a similar dependence on the Ta thickness, if one excludes the thinnest Ta layer, which might be discontinuous or oxidized, and thus exhibits a very large resistance ($R = 95$ k Ω is out of range of the graph).

To analyze the thickness dependence of the inverse spin Hall voltage, we follow the approach derived in Ref. 17. The spin diffusion equation with the appropriate source term and boundary conditions leads to the following expression:

$$V_{ISH} = \Theta_{SH} \frac{G_{\uparrow\downarrow}}{G_{\uparrow\downarrow} + \frac{\sigma}{\lambda_{sd}} \frac{1 - \exp(-2t_{NM}/\lambda_{sd})}{1 + \exp(-2t_{NM}/\lambda_{sd})}} \times \frac{hLPf \sin^2(\theta) [1 - \exp(-t_{NM}/\lambda_{sd})]^2}{2et_{NM} [1 + \exp(-2t_{NM}/\lambda_{sd})]}, \quad (2)$$

where σ is the conductivity of the normal metal, t_{NM} is its thickness, L is the length of the YIG|NM slab excited at frequency f by the microwave field, θ is the angle of precession of YIG, and P is an ellipticity correction factor. The latter depends on the excitation frequency¹⁸ and, in our case, $P \simeq 1.25$.

From Eq. (2), one can see that the *amplitude* of V_{ISH} depends on the transport parameters λ_{sd} , $G_{\uparrow\downarrow}$, and Θ_{SH} , as well as on the resonant precession angle θ . We do not have a direct measurement of θ , but it can be evaluated from the strength of the microwave field h_{rf} and the measured linewidth ΔH .³⁰ By performing network analyzer measurements and considering the geometry of the transmission line, we estimate the strength of the microwave field $h_{rf} \simeq 0.2$ Oe for a $P = +10$ dBm output power from the synthesizer. For the series of YIG|Ta samples, it yields a precession angle $\theta \simeq 3.3^\circ$ in YIG at 3.8 GHz.

Nevertheless, the measurements presented in Fig. 3 are not sufficient to extract independently $G_{\uparrow\downarrow}$ and Θ_{SH} .

The *thickness dependence* of V_{ISH} primarily depends on λ_{sd} , through the argument of the exponential functions in Eq. (2). The spin diffusion length can thus be adjusted to fit the shape of V_{ISH} vs. t_{Ta} in Fig. 3. The series of lines in Fig. 3 displays the result of calculations based on Eq. (2) for three different values of λ_{sd} , using the thickness dependent conductivity σ^{Ta} measured experimentally. A very good overall agreement to the data is found for a spin diffusion length $\lambda_{sd}^{Ta} = 1.8$ nm. We explain the discrepancy observed at $t_{Ta} = 1.5$ nm at which the measured voltage is about five times smaller than predicted, by the fact that the thinnest Ta layer is discontinuous or oxidized, as already pointed out.

C. Magnetoresistance: YIG|Pt versus YIG|Ta

We now turn to the measurements of dc magnetoresistance in our hybrid YIG|NM bilayers. We have measured the variation of resistance in the exact same samples as the ones studied by ISHE in Fig. 2, YIG|Pt (15 nm) and YIG|Ta (3 nm), as a function of the angle of the applied field with respect to the three main axes of the slabs. In these experiments, the applied field was fixed to $H = 3$ kOe (sufficient to saturate the YIG), and a dc current of a few mA together with a 6^{1/2} digits voltmeter were used to probe the resistance of the NM layers in a four-probe configuration. The results obtained by rotating the magnetic field in the plane of the sample (angle α), from in-plane perpendicular to the charge current J_e to out-of-plane (angle β) and from in-plane parallel to J_e to out-of-plane (angle γ) are presented in Figs. 4(a)–4(c), respectively (see also associated sketches).

In both YIG|Pt and YIG|Ta bilayers, we do observe a weak magnetoresistance ($\Delta R_{max}/R_0$ of 5×10^{-5} and 4×10^{-5} , respectively), as it was reported on the YIG|Pt system.²² We checked that this weak variation does not depend on the sign or strength of the probing current. In contrast to the inverse spin Hall voltage measurements presented in Fig. 2, we also note that the sign (or symmetry) of the effect is identical in YIG|Pt and YIG|Ta.

In order to interpret this magnetoresistance, it is important to understand its dependence on all three different angles, α , β , and γ , shown in Fig. 4. If one would just look at the in-plane behavior [see Fig. 4(a)], one could conclude that the NM resistance R changes according to some anisotropic magnetoresistance (AMR) effect, as if the NM would be magnetized at the interface with YIG due to proximity effect.²² But with AMR, R depends on the angle between the charge current J_e and the magnetization (applied field H). Hence no change of R is expected with the angle β , whereas R should vary with the angle γ , which is exactly opposite to what is observed in Figs. 4(b) and 4(c), respectively. Therefore usual AMR as the origin of the magnetoresistance in YIG|Pt and YIG|Ta bilayers has to be excluded.

Instead, the spin Hall magnetoresistance (SMR) mechanism proposed in Ref. 8 is well supported by our magnetoresistance data. In this scenario, the electrons carried by the charge current in the NM layer are deflected by SHE in opposite directions depending on their spin. Those whose spin is flipped by scattering at the interface with the FM can oppose the

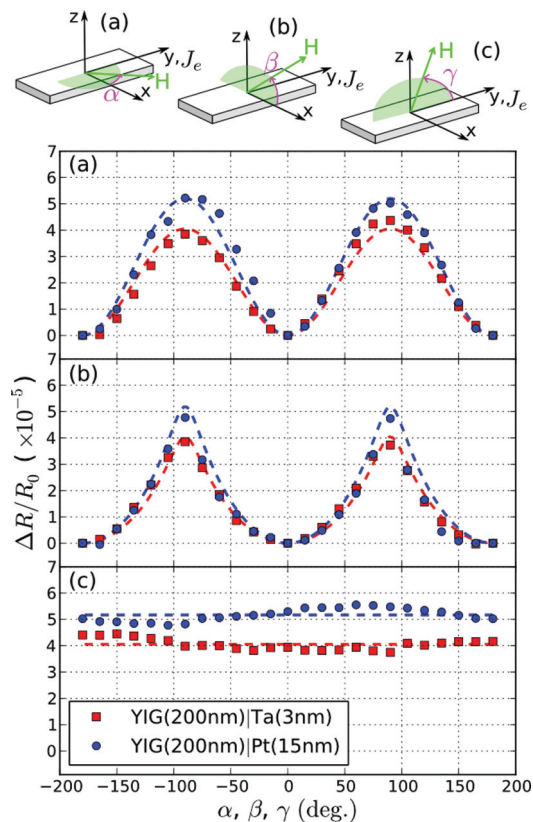


FIG. 4. (Color online) (a)–(c) Magnetoresistance in YIG|Ta and YIG|Pt as a function of the angle of the applied field ($H = 3$ kOe) sketched at the top (the samples are the same as the ones measured in Fig. 2). Dashed lines are predictions from Eq. (3) of the SMR theory (see Ref. 8).

initial current by ISHE and lead to an increase of resistance. Therefore the spin Hall magnetoresistance depends on the relative angle between the magnetization \mathbf{M} of the FM and the accumulated spins \mathbf{s} at the FM|NM interface:

$$R = R_0 + \Delta R_{\max} \sin^2(\mathbf{M}, \mathbf{s}). \quad (3)$$

The increase of resistance is maximal when \mathbf{M} and \mathbf{s} are perpendicular, because the spin-flip scattering governed by $G_{\uparrow\downarrow}$ at the interface is the largest. In the geometry depicted in Fig. 4, the charge current is applied along y , hence the spins accumulated at the YIG|NM interface due to SHE are oriented along x . The dashed lines plotted in Figs. 4(a)–4(c) are the prediction of the SMR theory. As can be seen, Eq. (3) explains the presence (absence) of resistance variation upon the applied field angles α and β (γ). Due to demagnetizing effects, the magnetization of YIG is not always aligned with the applied field. This is the reason why the measured curves in Figs. 4(a) and 4(b) have different shapes, and a simple calculation³⁰ of the equilibrium position of \mathbf{M} in combination with Eq. (3) reproduces them quite well.

The SMR ratio was also calculated in Ref. 8:

$$\text{SMR} = \frac{\Delta R_{\max}}{R_0} = \Theta_{\text{SH}}^2 \frac{2\lambda_{\text{sd}}^2}{\sigma_{\text{NM}}} G_{\uparrow\downarrow} \tanh^2\left(\frac{t_{\text{NM}}}{2\lambda_{\text{sd}}}\right) \frac{1}{1 + \frac{2\lambda_{\text{sd}}}{\sigma} G_{\uparrow\downarrow} \coth\left(\frac{t_{\text{NM}}}{\lambda_{\text{sd}}}\right)}. \quad (4)$$

As for the inverse spin Hall voltage V_{ISH} [see Eq. (2)], the SMR depends on all the transport parameters $G_{\uparrow\downarrow}$, Θ_{SH} , and

λ_{sd} , which therefore cannot be extracted individually from a single measurement. In Sec. IV A, we will take advantage of the combined measurements of V_{ISH} (see Figs. 2 and 3) and SMR (see Fig. 4) to do so. For now, it is interesting to point out that because both SHE and ISHE are at play in spin Hall magnetoresistance, the SMR depends on the *square* of the spin Hall angle. This explains the positive SMR for both YIG|Pt and YIG|Ta, even though the spin Hall angles of Pt and Ta are opposite.

Finally, it would have been interesting to measure the dependence of SMR on Ta thickness (the dependence on Pt thickness was studied in Refs. 22 and 29). Unfortunately, it was difficult to realize low noise four-point contacts to investigate the faint magnetoresistance on the series of Ta samples prepared to study V_{ISH} versus t_{Ta} . From our attempts, we found that the SMR of YIG|Ta (10 nm) is less than 2×10^{-5} . This is consistent with the decrease predicted by Eq. (4) (assuming $\lambda_{\text{sd}}^{\text{Ta}} = 1.8$ nm) with respect to the SMR $\simeq 4 \times 10^{-5}$ measured for YIG|Ta (3 nm).

IV. DISCUSSION

A. Transport parameters

As already discussed, both V_{ISH} and SMR depend on the set of transport parameters ($G_{\uparrow\downarrow}$, Θ_{SH} , λ_{sd}). By studying V_{ISH} as a function of the NM thickness, the spin diffusion length can be determined, and we found that in Ta, $\lambda_{\text{sd}}^{\text{Ta}} = 1.8 \pm 0.7$ nm, see Fig. 3. We mention here that from a similar study on YIG|Pt, $\lambda_{\text{sd}}^{\text{Pt}} = 3.0 \pm 0.5$ nm could be inferred.¹⁷ This value lies in the range of spin diffusion lengths reported on Pt, which span over almost an order of magnitude,²⁶ from slightly more than 1 nm up to 10 nm.

We note that the spin diffusion length extracted from the YIG|Ta data of Fig. 3 is somewhat shorter than the 2.7 nm inferred from nonlocal spin-valve measurements.²³ The value found for the spin diffusion length in Ta is short, but reasonable as it represents several times the electronic mean free paths, which are of the order of 0.4 nm. We note here that indeed Ta is very resistive but still in the metallic-like regime with sheet resistances below 4 k Ω . However, the extraction of physical spin diffusion lengths in these measurements is at the heart of a present controversy.²⁶ It seems indeed that nonlocal measurements give systematically larger values than those extracted from ISHE measurements of FMR spin pumping. In this respect, we would like to point out that perhaps the model of Eq. (2) is too simple for the present problem as charge current (for resistivity measurements) and spin currents are in two different directions: the former is in-plane while the latter is perpendicular to the plane. Hence the spin current has to cross one interface and interacts with the free surface of the metallic layer. It is not clear to us that the relevant quantity in the problem is really the bulk λ_{sd} . It is not impossible that the relevant spin diffusion length also depends on layer thickness, but this refinement is beyond the reach of the present paper.

There is a direct way to get the spin mixing conductance of a FM|NM interface, by determining the increase of damping in the FM layer associated to spin pumping in the adjacent NM layer.⁷ Due to its interfacial nature, this effect is inversely proportional to the thickness of the FM

TABLE I. Transport parameters obtained from the analysis of inverse spin Hall voltage [Figs. 2 and 3 + Eq. (2)] and spin Hall magnetoresistance [Fig. 4 + Eq. (4)] performed on YIG|Ta (1.5–15 nm) and YIG|Pt (15 nm).

	YIG Ta (1.5–15 nm)	YIG Pt (15 nm)
σ ($10^6 \Omega^{-1} \text{m}^{-1}$)	0.08–0.75	2.45 ± 0.10
λ_{sd} (10^{-9}m)	1.8 ± 0.7	n/a [from 1.5 to 10] ²⁶
$G_{\uparrow\downarrow}$ ($10^{13} \Omega^{-1} \text{m}^{-2}$)	$4.3 \pm_{-2}^{+11}$	$6.2 \pm_{-4}^{+14}$
Θ_{SH}	$-0.02 \pm_{-0.015}^{+0.008}$	$0.03 \pm_{-0.015}^{+0.04}$

and can be measured only on ultrathin films. This was recently achieved in nanometer-thick YIG films grown by pulsed laser deposition,^{31,32} where spin mixing conductances $G_{\uparrow\downarrow} = (0.7\text{--}3.5) \times 10^{14} \Omega^{-1} \text{m}^{-2}$ have been reported for the YIG|Au interface.

Even for 200-nm-thick YIG films as ours, it is possible to obtain the full set of transport parameters thanks to our combined measurements of V_{ISH} and SMR on YIG|NM hybrid structures. In fact, from Eqs. (2) and (4), the ratio $V_{\text{ISH}}^2/\text{SMR}$ does not depend on Θ_{SH} , which allows to determine $G_{\uparrow\downarrow}$. Then, the last unknown Θ_{SH} can be found from the V_{ISH} or SMR signal. This is how we proceed to determine the transport parameters, which are collected in Table I. The drawback of this method is that it critically relies on (i) λ_{sd} , which enters in the argument of exponential functions in Eqs. (2) and (4) and (ii) the angle of precession θ in the inverse spin Hall experiment, since $V_{\text{ISH}}^2/\text{SMR} \propto \theta^4$. Our estimation of θ being within $\pm 25\%$, the value extracted for $G_{\uparrow\downarrow}$ from the ratio $V_{\text{ISH}}^2/\text{SMR}$ can vary by a factor up to 8 due to this uncertainty. The spin Hall angle Θ_{SH} is less sensitive to other parameters, still it can vary by a factor up to 3. This explains the rather large error bars in Table I. In this study, we did not determine the spin diffusion length in Pt, hence we used the range of values reported in the literature.²⁶

The spin mixing conductances determined from our combined V_{ISH} and SMR measurements on YIG|Ta and YIG|Pt bilayers lie in the same window as the ones determined from interfacial increase of damping in YIG|Au,³¹ from inverse spin Hall voltage in BiY₂Fe₅O₁₂|Au and Pt,³³ and from first-principles calculations in YIG|Ag.²⁵ We would like to point out that despite the large uncertainty, $G_{\uparrow\downarrow}$ for YIG|Ta is likely less than for YIG|Pt. We note that the smaller damping measured in CoFeB|Ta compared to CoFeB|Pt was tentatively attributed to a smaller spin mixing conductance.²⁰

The spin Hall angles that we report for Pt and Ta are both of a few percents. In particular, $\Theta_{\text{SH}}^{\text{Ta}} \simeq -0.02$ lies in between the values determined from nonlocal spin-valve measurements ($\simeq -0.004$)²³ and from spin-torque switching using the SHE ($\simeq -0.12$).²⁰

The main conclusion, which arises from the summary presented in Table I, is that the sets of transport parameters determined for the hybrid YIG|Ta and YIG|Pt systems are quite similar. Apart from the opposite sign of Θ_{SH} in Ta and Pt, the main difference concerns the conductivity: $\sigma^{\beta\text{-Ta}}$ is roughly one order of magnitude smaller than σ^{Pt} . This explains the large inverse spin Hall voltages that can be detected in our YIG|Ta bilayers (up to 70 μV at $P = +10$ dBm), since from Eq. (2) $V_{\text{ISH}} \propto 1/\sigma$, which could be a useful feature of the Ta layer.

B. Influence of a dc current on FMR linewidth

Onsager reciprocal relations imply that if there is an ISHE voltage produced by the precession of YIG, there must also be a transfer of spin angular momentum from the NM conduction electrons to the magnetization of YIG, through the finite spin mixing conductance at the YIG|NM interface.²⁵ Therefore one would expect to be able to control the relaxation of the insulating YIG by injecting a dc current in an adjacent strong spin-orbit metal, as it was shown on YIG|Pt in the pioneering work of Kajiwara *et al.*⁶ Although this direct effect is well established when the ferromagnetic layer is ultra-thin and metallic,^{34–37} only a few works report on conclusive effects on micron-thick YIG^{6,38,39} or provide a theoretical interpretation to the phenomenon.⁴⁰

The 200-nm-thick YIG films that have been grown for this study are about six times thinner than the one used in Ref. 6, with an intrinsic relaxation close to bulk YIG. Because the spin transfer torque is an interfacial effect and sizable spin mixing conductances have been measured in our YIG|Ta and YIG|Pt bilayers, our samples must be good candidates to observe the direct effect of a dc current on the relaxation of YIG. Due to their large resistance, β -Ta films are not convenient to pass the large current densities required to observe such an effect (large Joule heating). Therefore we have conducted these experiments only on the YIG|Pt films prepared in this work.

The inverse spin Hall voltage measurements presented in Fig. 2 have therefore been repeated in the presence of a dc current flowing through the Pt layer. This type of experiment, where a ferromagnetic layer is excited by a small amplitude signal and a spin polarized current can influence the linewidth of the resonance, has already been reported on spin-valve spin-torque oscillators^{41,42} and NiFe|Pt bilayers.^{35,43} The results obtained on our YIG (200 nm)|Pt (15 nm) at 77 K when the dc current is varied from -40 to $+40$ mA are displayed in Fig. 5.

Let us now comment on these experiments. We first emphasize that the current injected in Pt is truly dc (not pulsed). A sizable Joule heating is thus induced, as reflected by the increase of Pt resistance. As a consequence, the main effect of dc current injection at room temperature is the displacement of the resonance towards larger field, due to the decrease of the YIG saturation magnetization M_s . To avoid this trivial effect, we have performed these experiments directly in liquid nitrogen. In that case, the increase of Pt resistance is very limited ($+0.2\%$ at ± 40 mA). We note that when cooled from 300 K down to 77 K, the peak of the inverse spin Hall voltage measured in the YIG|Pt bilayer is displaced towards lower field due to the increase of M_s of YIG (from 140 to 200 emu/cm³), and its amplitude slightly decreases.

The main conclusion that can be drawn from Fig. 5 is that there is basically no effect of the dc current injected in Pt on the YIG resonance. We stress that the maximal current density reached in Pt in these experiments is $J_e = 2.4 \times 10^9 \text{ A m}^{-2}$, i.e., twice larger than the one at which YIG magnetization oscillations were reported in Ref. 6. In our experiments, we are not looking for auto-oscillations of YIG, which requires that the damping is fully compensated by spin transfer torque, but only for some variation of the linewidth. The fact that we do not see any change in the shape of the resonant peak of

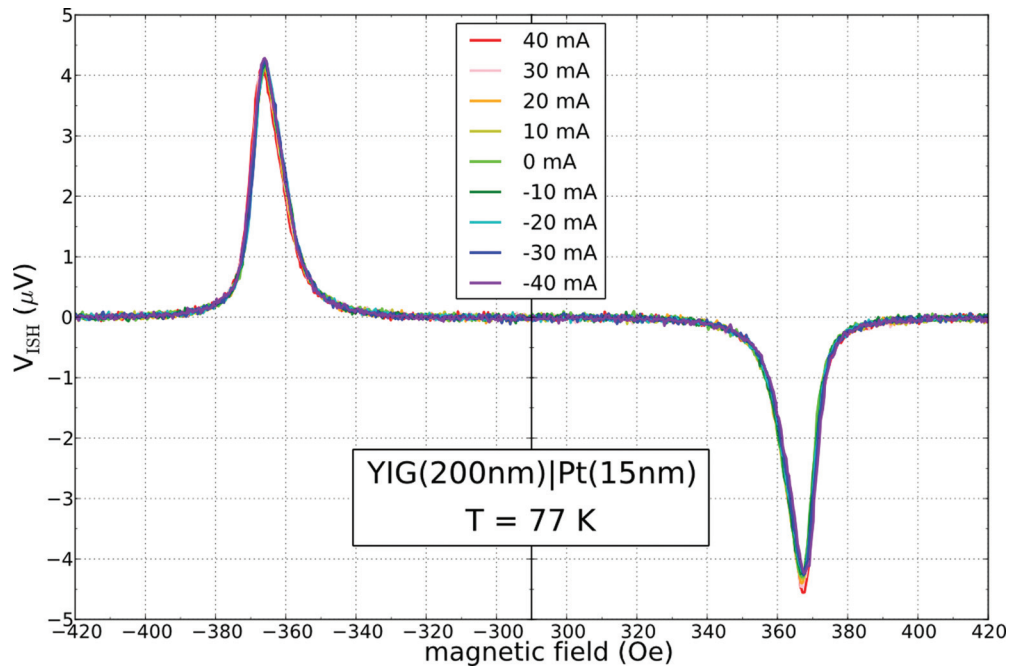


FIG. 5. (Color online) Inverse spin Hall voltage measured at 2.95 GHz ($P = +10$ dBm) for YIG|Pt as a function of the dc current flowing in the Pt layer. A small current dependent offset ($<0.2 \mu\text{V}$) has been subtracted to the data.

our 200-nm-thin YIG film is thus in contradiction with the observation of bulk auto-oscillations in thicker films.⁶

We have also performed similar experiments on the other YIG(200 nm)|Pt samples, which were prepared using the two different YIG films grown for this study. Although the current density was increased up to $6 \times 10^9 \text{ A m}^{-2}$, we were never able to detect any sizable variation of the linewidth of YIG. Instead, we have measured that the dc current can affect the inverse spin Hall voltage in different ways. First, when a charge current is injected into Pt, a non-zero offset of the lock-in signal can be detected (it was subtracted in Fig. 5). This is due to the increase of Pt resistance induced by the microwave power, as it was verified by monitoring this offset while varying the modulation frequency of the microwave. Secondly, the amplitude of the V_{ISH} peaks can be affected by the dc current (but again, *not* the linewidth). This effect can at first be confused with some influence on the relaxation of YIG, because it displays the appropriate symmetries versus field and current. But instead, we have found that this is a bolometric effect:⁴⁴ when the YIG is excited at resonance, it heats up, thereby heating the adjacent Pt whose resistance gets slightly larger. Hence an additional voltage to V_{ISH} is picked up on the lock-in due to the nonzero dc current flowing in Pt. Therefore, one should be very careful in interpreting changes in inverse spin Hall voltage as the indication of damping variation in YIG. Finally, we observed that at very large current density, the resonance peak slightly shifts towards larger field due to Joule heating, even at 77 K.

V. CONCLUSION

In this paper, we have presented and analyzed a comparative set of data of inverse spin Hall voltage V_{ISH} and

magnetoresistance obtained on YIG|Pt and YIG|Ta bilayers. We have detected the voltages generated by spin pumping at the YIG|Pt interface (already well established)⁶ and at the YIG|Ta interface. Their opposite signs are assigned to the opposite spin Hall angles in Pt and Ta.²⁴ From the thickness dependence of V_{ISH} , we have been able to obtain the spin diffusion length in Ta, $\lambda_{\text{sd}}^{\text{Ta}} = 1.8 \pm 0.7 \text{ nm}$, in reasonable agreement with the value extracted from nonlocal spin valve measurements.²³ From symmetry arguments, we have shown that the weak magnetoresistance measured on our hybrid YIG|NM layers cannot be attributed to usual AMR, but is instead well understood in the framework of the recently introduced spin Hall magnetoresistance (SMR).⁸ By taking advantage of the combined measurements of V_{ISH} and SMR performed on the same samples, we have been able to extract the spin Hall angles in Pt and Ta, as well as the spin mixing conductances at the YIG|Pt and YIG|Ta interfaces.

These transport parameters have all been found to be of the same order of magnitude as those already measured^{20,31} or predicted.²⁵ We believe that at least part of the discrepancies between the parameters evaluated in different works²⁶ depend on the details of the YIG|NM interface³² and on the quality of the NM.^{18,19,23}

Finally, we could not detect any change of linewidth in our YIG|Pt samples by passing large current densities through the Pt layer. One might argue that our high-quality 200-nm YIG thin films are still too thick to observe any appreciable effect of spin transfer torque, which is an interfacial mechanism, or that the spin-waves which can auto-oscillate under the action of spin transfer at the interface with Pt are different from the uniform mode that we excite with the microwave field in our experiments.^{6,40} If one would estimate the threshold current required to fully compensate the damping of all the

magnetic moments contained in our YIG films,^{20,40} $J_{\text{th}} \simeq 2e\alpha\omega M_s t_{\text{YIG}} / (\Theta_{\text{SH}} \gamma \hbar)$, one would get current densities of about 10^{11} A m⁻². This is 20 times larger than the largest current density which we have tried. Thus the lack of a visible effect in our Fig. 5 is not a real surprise in itself, but it is inconsistent with the results reported in Ref. 6. Future experiments on ultrathin YIG|NM hybrid films, in which the

spin mixing conductance can be directly determined from the interfacial increase of damping,³¹ might give a definite answer to this point.

ACKNOWLEDGMENT

This research was supported by the French ANR Grant Trinidad (ASTRID 2012 program).

*Corresponding author: gregoire.deloubens@cea.fr

¹M. I. Dyakonov and V. I. Perel, *JETP Lett.* **13**, 467 (1971).

²J. E. Hirsch, *Phys. Rev. Lett.* **83**, 1834 (1999).

³S. O. Valenzuela and M. Tinkham, *Nature (London)* **442**, 176 (2006).

⁴T. Kimura, Y. Otani, T. Sato, S. Takahashi, and S. Maekawa, *Phys. Rev. Lett.* **98**, 156601 (2007).

⁵E. Saitoh, M. Ueda, H. Miyajima, and G. Tatara, *Appl. Phys. Lett.* **88**, 182509 (2006).

⁶Y. Kajiwara, K. Harii, S. Takahashi, J. Ohe, K. Uchida, M. Mizuguchi, H. Umezawa, H. Kawai, K. Ando, K. Takanashi, S. Maekawa, and E. Saitoh, *Nature (London)* **464**, 262 (2010).

⁷Y. Tserkovnyak, A. Brataas, G. E. W. Bauer, and B. I. Halperin, *Rev. Mod. Phys.* **77**, 1375 (2005).

⁸H. Nakayama, M. Althammer, Y.-T. Chen, K. Uchida, Y. Kajiwara, D. Kikuchi, T. Ohtani, S. Geprags, M. Opel, S. Takahashi, R. Gross, G. E. W. Bauer, S. T. B. Goennenwein, and E. Saitoh, arXiv:1211.0098.

⁹K. Ando, Y. Kajiwara, S. Takahashi, S. Maekawa, K. Takemoto, M. Takatsu, and E. Saitoh, *Phys. Rev. B* **78**, 014413 (2008).

¹⁰A. Azevedo, L. H. Vilela-Leˆao, R. L. Rodrıguez-Suarez, A. F. Lacerda Santos, and S. M. Rezende, *Phys. Rev. B* **83**, 144402 (2011).

¹¹Z. Feng, J. Hu, L. Sun, B. You, D. Wu, J. Du, W. Zhang, A. Hu, Y. Yang, D. M. Tang, B. S. Zhang, and H. F. Ding, *Phys. Rev. B* **85**, 214423 (2012).

¹²O. Rousseau and M. Viret, *Phys. Rev. B* **85**, 144413 (2012).

¹³C. W. Sandweg, Y. Kajiwara, K. Ando, E. Saitoh, and B. Hillebrands, *Appl. Phys. Lett.* **97**, 252504 (2010).

¹⁴H. Kurebayashi, O. Dzyapko, V. E. Demidov, D. Fang, A. J. Ferguson, and S. O. Demokritov, *Nat. Mater.* **10**, 660 (2011).

¹⁵L. H. Vilela-Leˆao, C. Salvador, A. Azevedo, and S. M. Rezende, *Appl. Phys. Lett.* **99**, 102505 (2011).

¹⁶A. V. Chumak, A. A. Serga, M. B. Jungfleisch, R. Neb, D. A. Bozhko, V. S. Tiberkevich, and B. Hillebrands, *Appl. Phys. Lett.* **100**, 082405 (2012).

¹⁷V. Castel, N. Vlietstra, J. Ben Youssef, and B. J. van Wees, *Appl. Phys. Lett.* **101**, 132414 (2012).

¹⁸O. Mosendz, V. Vlaminc, J. E. Pearson, F. Y. Fradin, G. E. W. Bauer, S. D. Bader, and A. Hoffmann, *Phys. Rev. B* **82**, 214403 (2010).

¹⁹K. Kondou, H. Sukegawa, S. Mitani, K. Tsukagoshi, and S. Kasai, *Appl. Phys. Express* **5**, 073002 (2012).

²⁰L. Liu, C.-F. Pai, Y. Li, H. W. Tseng, D. C. Ralph, and R. A. Buhrman, *Science* **336**, 555 (2012).

²¹C.-F. Pai, L. Liu, Y. Li, H. W. Tseng, D. C. Ralph, and R. A. Buhrman, *Appl. Phys. Lett.* **101**, 122404 (2012).

²²S. Y. Huang, X. Fan, D. Qu, Y. P. Chen, W. G. Wang, J. Wu, T. Y. Chen, J. Q. Xiao, and C. L. Chien, *Phys. Rev. Lett.* **109**, 107204 (2012).

²³M. Morota, Y. Niimi, K. Ohnishi, D. H. Wei, T. Tanaka, H. Kontani, T. Kimura, and Y. Otani, *Phys. Rev. B* **83**, 174405 (2011).

²⁴T. Tanaka, H. Kontani, M. Naito, T. Naito, D. S. Hirashima, K. Yamada, and J. Inoue, *Phys. Rev. B* **77**, 165117 (2008).

²⁵X. Jia, K. Liu, K. Xia, and G. E. W. Bauer, *Europhys. Lett.* **96**, 17005 (2011).

²⁶L. Liu, R. A. Buhrman, and D. C. Ralph, arXiv:1111.3702v3.

²⁷V. Castel, N. Vlietstra, B. J. van Wees, and J. Ben Youssef, *Phys. Rev. B* **86**, 134419 (2012).

²⁸R. Hoogeveen, M. Moske, H. Geisler, and K. Samwer, *Thin Solid Films* **275**, 203 (1996).

²⁹N. Vlietstra, J. Shan, V. Castel, J. Ben Youssef, and B. J. van Wees, arXiv:1301.3266.

³⁰A. G. Gurevich and G. A. Melkov, *Magnetization Oscillations and Waves* (CRC Press, Boca Raton, FL, 1996).

³¹B. Heinrich, C. Burrowes, E. Montoya, B. Kardasz, E. Girt, Y.-Y. Song, Y. Sun, and M. Wu, *Phys. Rev. Lett.* **107**, 066604 (2011).

³²C. Burrowes, B. Heinrich, B. Kardasz, E. A. Montoya, E. Girt, Y. Sun, Y.-Y. Song, and M. Wu, *Appl. Phys. Lett.* **100**, 092403 (2012).

³³R. Takahashi, R. Iguchi, K. Ando, H. Nakayama, T. Yoshino, and E. Saitoh, *J. Appl. Phys.* **111**, 07C307 (2012).

³⁴K. Ando, S. Takahashi, K. Harii, K. Sasage, J. Ieda, S. Maekawa, and E. Saitoh, *Phys. Rev. Lett.* **101**, 036601 (2008).

³⁵V. E. Demidov, S. Urazhdin, E. R. J. Edwards, M. D. Stiles, R. D. McMichael, and S. O. Demokritov, *Phys. Rev. Lett.* **107**, 107204 (2011).

³⁶V. E. Demidov, S. Urazhdin, H. Ulrichs, V. Tiberkevich, A. Slavin, D. Baither, G. Schmitz, and S. O. Demokritov, *Nat. Mater.* **11**, 1028 (2012).

³⁷L. Liu, C.-F. Pai, D. C. Ralph, and R. A. Buhrman, *Phys. Rev. Lett.* **109**, 186602 (2012).

³⁸Z. Wang, Y. Sun, M. Wu, V. Tiberkevich, and A. Slavin, *Phys. Rev. Lett.* **107**, 146602 (2011).

³⁹E. Padron-Hernandez, A. Azevedo, and S. M. Rezende, *Appl. Phys. Lett.* **99**, 192511 (2011).

⁴⁰J. Xiao and G. E. W. Bauer, *Phys. Rev. Lett.* **108**, 217204 (2012).

⁴¹J. C. Sankey, P. M. Braganca, A. G. F. Garcia, I. N. Krivorotov, R. A. Buhrman, and D. C. Ralph, *Phys. Rev. Lett.* **96**, 227601 (2006).

⁴²W. Chen, J.-M. L. Beaujour, G. de Loubens, A. D. Kent, and J. Z. Sun, *Appl. Phys. Lett.* **92**, 012507 (2008).

⁴³L. Liu, T. Moriyama, D. C. Ralph, and R. A. Buhrman, *Phys. Rev. Lett.* **106**, 036601 (2011).

⁴⁴Y. S. Gui, N. Mecking, A. Wirthmann, L. H. Bai, and C.-M. Hu, *Appl. Phys. Lett.* **91**, 082503 (2007).